scientific reports

Check for updates

OPEN

Solar cell design using graphene-based hollow nano-pillars

Shiva Hayati Raad✉ & Zahra Atlasbaf

In this paper, the full solar spectrum coverage with an absorption efficiency above 96% is attained by shell-shaped graphene-based hollow nano-pillars on top of the refractory metal substrate. The material choice guarantees the high thermal stability of the device along with its robustness against harsh environmental conditions. To design the structure, constitutive parameters of graphene material in the desired frequency range are investigated and its absorption capability is illustrated by calculating the attenuation constant of the electromagnetic wave. It is observed that broadband absorption is a consequence of wideband retrieved surface impedance matching with the free-space intrinsic impedance due to the tapered geometry. Moreover, the azimuthal and longitudinal cavity resonances with different orders are exhibited for a better understanding of the underlying wideband absorption mechanism. Importantly, the device can tolerate the oblique incidence in a wide span around 65°, regardless of the polarization. The proposed structure can be realized by large-area fabrication techniques.

Solar energy trapping, as the main source of renewable energy, has been the focus of extensive research for many years[1]. For this purpose, different geometrical and material combinations have been proposed, only some of them covering the whole spectrum. For instance, the relatively poor absorption efficiency of thin-film solar cells is the consequence of the indirect bandgap of silicon, where surface plasmon resonances of metallic nanoparticles can be used to enhance it[2,3]. In these solar cells, prolonged action of air and moisture affect the photocurrent generation due to the formation of oxide layers on metallic particles[4]. As an alternative approach, the front-sided integration of high-index dielectric particles has been proposed to enhance the power conversion efficiency of the thin-film solar cells[5]. Metasurface-based absorbers are another common category of solar cells, where metal–insulator-–metal (MIM) stacks have been widely used. In the aforementioned solar thermo-photovoltaic systems (STPV), the proper choice of the metal (rather than using noble metals) to withstand high temperature is a key factor[6]. Refractory metals, possibly coated with protection layers, are good candidates for this purpose because of their heat-tolerant and large absorption capabilities[7–9].

Because of their broadband absorption nature, excellent chemical stability, high thermal stability, and excellent thermal conductivity, carbon-based materials have gained lots of interest as photo-thermal materials[10,11]. In this regard, a graphene\semiconductor heterostructure has been proposed for stable and efficient conversion of the light to electricity, being much thinner than its commercial silicon p–n junction counterparts[12]. Moreover, silicon photovoltaics can benefit from graphene as a semi-transparent electrode and an antireflection coating[13]. As another instance, by integrating Al nanoparticles and wrinkle-like graphene sheets, 7.2% enhancement in the photocurrent density of the solar cell is attained[14]. Moreover, broadband absorption of the un-polarized light is achieved using a 90-nm graphene dielectric stack which behaves as a hyperbolic metamaterial[15]. The aim of the present research is the design of a graphene-based ultra-broadband absorber covering the whole solar spectrum. A comprehensive review of graphene synthesis and functionalization for solar cells can be found in[16].

Ultra-broadband absorbers can be realized using different approaches. Combined narrowband resonances to form super-unit, multi-resonance structures, and multi-layered configurations are beneficial for resonant devices[17]. In the non-resonant approach, the wideband absorption is the consequence of gradient impedance matching, and the energy is dissipated either in lossy conductors or lossy dielectrics[18]. For instance, in the Sierpinski carpet, MIM absorber, and metallic nano-wires filled pyramid dielectric medium absorber, the absorption spectrum is widened by merging multiple resonances[19,20]. The absorption enhancement mechanism of the wideband truncated-pyramid-based metamaterial absorber and truncated titanium/semiconductor cone absorber can be respectively understood by extracting the effective impedance and Fabry–Perot cavity like resonances of

Department of Electrical and Computer Engineering, Tarbiat Modares University, Tehran, Iran. ✉email: shiva.hayati@modares.ac.ir

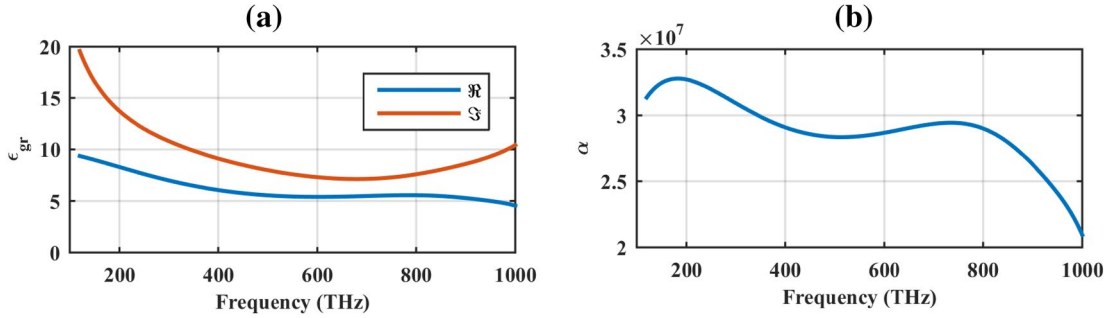

Figure 1. (**a**) Real and imaginary parts of graphene equivalent permittivity in the solar spectrum and (**b**) its attenuation constant.

the high-index dielectric resonator[21,22]. Due to the inherent wideband nature of tapered structures, in the paper, the cone-shaped geometry is chosen as the building block and its absorption spectrum is further manipulated by truncating the tip and hollowing the nano-pillars. In the following paragraphs, after wisely choosing the materials, the optical performance of the shell-shaped truncated hollow cone solar cell will be discussed in detail. The paper is organized as follows. At first, the potential of graphene material in the solar cell design is investigated by introducing its constitutive parameters. Later, the attenuation constant of the electromagnetic wave illuminated to the graphene slab is calculated to confirm its absorption capability. Finally, using a shell-shaped graphene-based nano-pillar and refractory metal substrate, respectively the impedance matching and transmission blockage conditions are satisfied in the desired spectrum. Multiple parametric studies are conducted to better understand the performance.

Results and discussions

In the following sections, the design procedure and performance analysis of a graphene-based solar cell is investigated in detail. After exhibiting the absorption capability of graphene material in the solar spectrum, by wideband impedance matching and transmission elimination, a full-spectrum solar cell is proposed and its performance is discussed employing multiple simulations.

Material choice. Let us initially investigate the equivalent permittivity of graphene material in the solar spectrum. The solar radiation covers the wavelength range of 295–2500 nm (~100–1200 THz), comprised of ultraviolet, visible, and infrared light[9]. In the infrared regime, graphene is commonly modeled by its surface conductivity calculated based on Kubo formulas. The outstanding feature of graphene in the plasmonic state is being reconfigurable through its chemical potential and relaxation time[23]. In this band, graphene surface conductivity can also be converted to the equivalent bulk permittivity with the negative real part using the Ampere's low[24]. In the visible spectrum and beyond, graphene behaves as an ordinary dielectric. Thus, the Drude Lorentz model can be used to approximate the monolayer graphene dispersive permittivity using the measured data[25]. Hence[26]:

$$\varepsilon_{gr} = \varepsilon_{\infty} - \frac{\omega_{gra}^2}{\omega^2 + i\omega\gamma_{gra}} + \sum_{j=1}^{m} \frac{\Delta\varepsilon_j \Omega_j^2}{\Omega_j^2 - \omega^2 - i\omega\Gamma_j} \tag{1}$$

where $m = 3$, $\varepsilon_{\infty} = 1.964$, $\Delta\varepsilon_j = (6.99,\ 1.69,\ 1.53)$, $\hbar\Gamma_j = (7.99,\ 2.01,\ 0.88)\,eV$, $\hbar\omega_{gra} = 6.02\,eV$, $\hbar\gamma_{gra} = 4.52\,eV$, $\hbar\Omega_j = (3.14,\ 4.03,\ 4.59)\,eV$. Figure 1a shows the real and imaginary parts of graphene permittivity in the solar spectrum, where relatively high real and imaginary parts are observed. In the next step, the attenuation constant of the illuminating wave to a graphene slab is studied to investigate whether the electromagnetic wave can penetrate it or not. The attenuation constant (Neper/meter) reads as[27]:

$$\alpha = \omega\sqrt{\varepsilon_0\mu_0}\left(a^2 + b^2\right)^{1/4} \sin\left(\frac{1}{2}\tan^{-1}\left(\frac{a}{b}\right)\right) \tag{2}$$

The parameters a and b in (2) are defined as: $a = \left(\varepsilon_r'\mu_r' - \varepsilon_r''\mu_r''\right)$ and $b = \left(\varepsilon_r'\mu_r'' + \varepsilon_r''\mu_r'\right)$. As Fig. 1b confirms, the graphene material has a large attenuation constant in the solar spectrum, making it suitable for the absorber design. Where prime and double prime respectively denote the real and imaginary parts of the permittivity (ε) and permeability (μ). Graphene is a non-magnetic material, therefore the real and imaginary parts of its permeability are respectively one and zero.

Proposing the device and performance analysis. The unit cell of our proposed absorber for the full coverage of the solar spectrum is illustrated in Fig. 2. This geometry is constructed by a refectory metal substrate, where its surface is covered by high aspect ratio graphene-based shell-shaped hollow nano-pillars. The height of the substrate and nano-pillars are considered $h_1 = 100$ nm and $h_2 = 1600$ nm, respectively. The dispersive permittivity of TiN refractory metal is extracted from[28,29] and that of the graphene is based on (1). The graphene nano-pillar is with a bottom radius of $R_1 = 120$ nm and a top radius of $R_2 = 40$ nm. Moreover, the periodicity

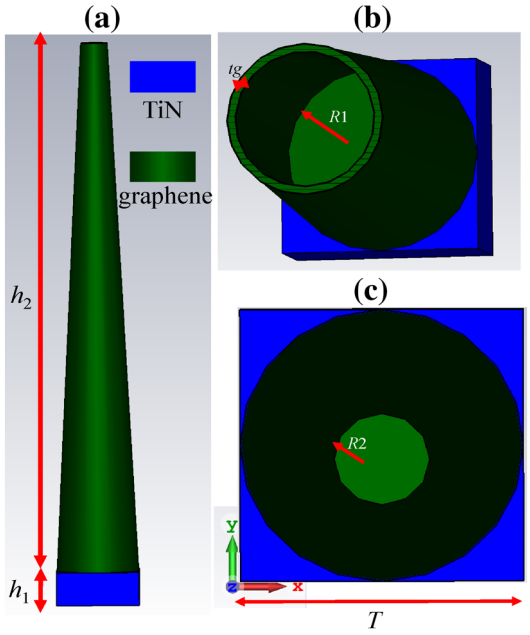

Figure 2. Unit cell of the proposed solar cell constructed by hollow graphene-based shell-shaped nano-pillars backed by a refractory metal (**a**) side view (**b**) top view for $h_2 = 500$ nm and (**c**) overall top view. The substrate and nano-pillar heights are respectively h_1 and h_2. The thickness of the graphene shell is denoted by t_g. Moreover, the bottom and top radii of the cone are R_1 and R_2 respectively. The periodicity of the nano-pillars in the square lattice is T.

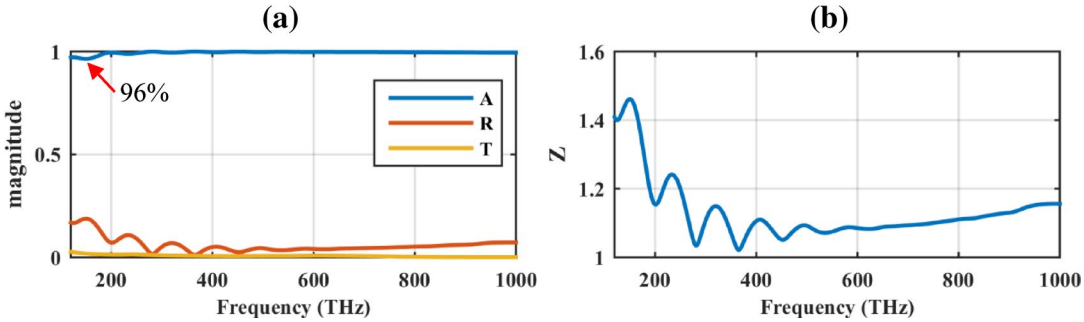

Figure 3. (**a**) The absorbance (A), reflectance (R), and transmittance (T) of the designed solar cell and (**b**) its retrieved surface impedance.

is $T = 2R_1 + p = 240$ nm ($p = 0$) and the thickness of the graphene shell is $t_g = 10$ nm. The dispersive permittivity introduced in (1) is used for the layered graphene as well[30]. Note that 3D nano-pillars can be fabricated by hole-mask colloidal lithography[31]. The method can also be used for the large-scale fabrication of shaped high index dielectric patterns[32]. Tape-assist transfer and spin coating can be used for wrapping graphene on curved surfaces[33–35]. Moreover, the core template can be removed by immersing it in hydrofluoric acid (HF) solution with stirring to reach ultrathin-shell graphene hollow particle[36].

As Fig. 3a shows, the achieved absorption rate is above 96% in the whole solar spectrum, being above 99% beyond 247 THz. Included in the figure are the reflectance and transmittance curves, showing a negligible amount of them. Moreover, the retrieved surface impedance is exhibited in Fig. 3b. The results are provided based on the simulated scattering parameters via[37]:

$$Z = \pm \frac{1 + S_{11}}{1 - S_{11}} \tag{3}$$

Based on the figure, wideband impedance matching is observed in this spectrum. The results of the above figures show that the underlying mechanism of the absorption is wideband impedance matching and transmission blockage[38]. The geometrical parameters are comparable with the TiN-shell based nano-pillar solar cell[31].

The spatial components of the electric field at three different frequencies (begin, middle, and end of the spectrum) are provided in Table 1. As the table indicates, azimuthal and longitudinal cavity resonances with

Frequency (THz)	E_x	E_y	E_z	
120	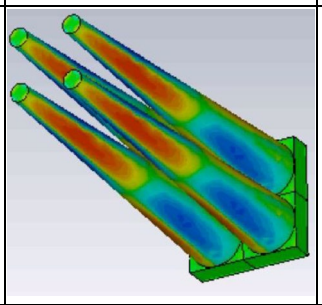	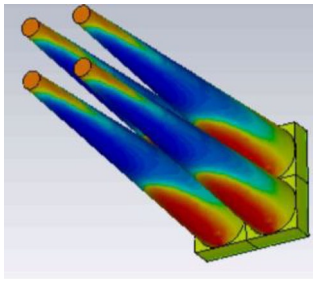	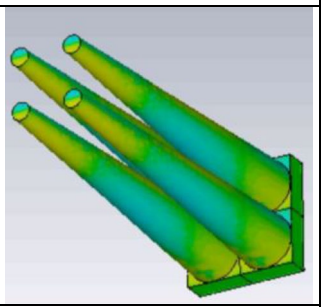	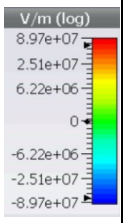
560	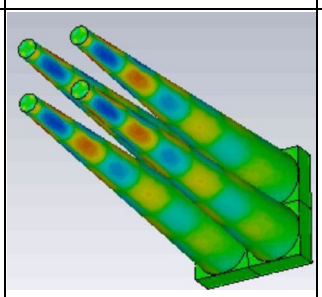	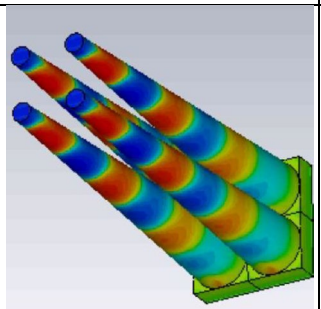	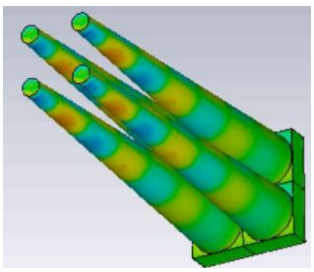	
1000	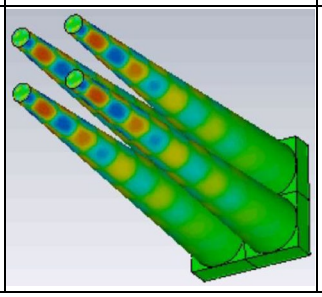	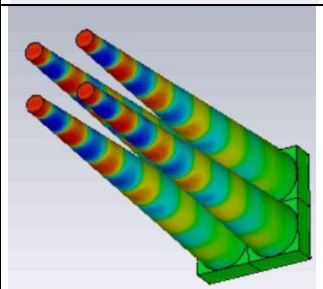	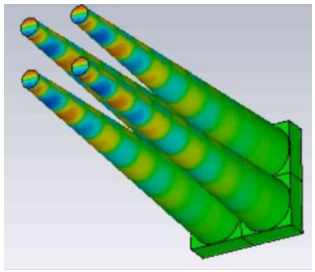	

Table 1. Spatial distribution of the electric field at three different frequencies.

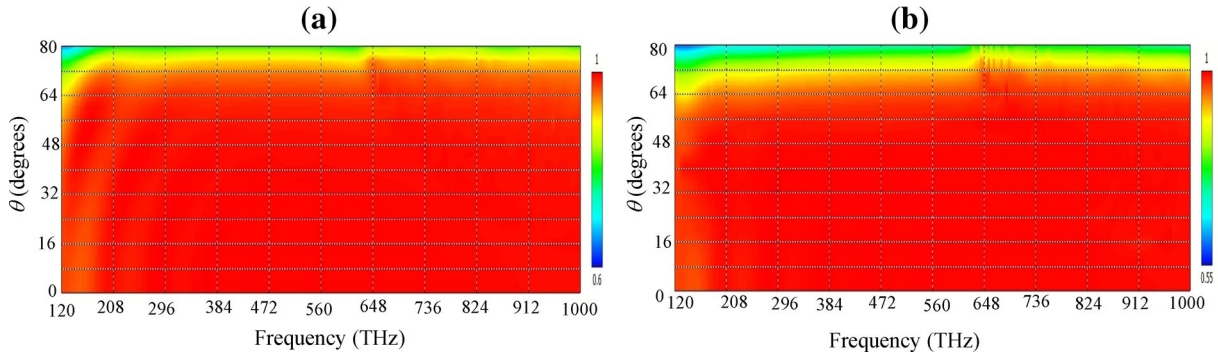

Figure 4. The sensitivity of the absorption spectrum to the incident angle for (**a**) TE and (**b**) TM waves.

different orders are responsible for the high absorption rate. The field distribution at the lower frequency edge shows that the height of the cone can be tuned based on the minimum frequency requirement. Note that although high aspect ratio micro-nano structures are realizable[39], the impact of the height on optical absorption is further discussed in the last section to reach geometrically compact devices for high-frequency operation.

The sensitivity of the absorption to the incident angle of the radiating wave is shown in Fig. 4 for TE and TM waves. The device has a polarization-insensitive response due to its four-fold symmetry[40] and the absorption rate above 90% can be attained for angles up to 65°.

Figure 5a shows the absorption rate of the proposed solar cell when the core is made of SiO_2 material with a refractive index of 1.45[9]. Based on the figure, the hollow nano-pillars have better low-frequency performance. Absorption rate enhancement by decreasing the core permittivity is expected since it is equivalent to the decrease

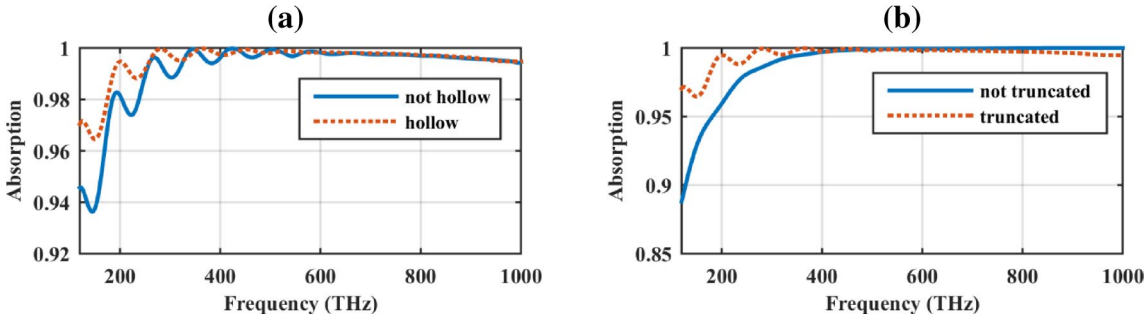

Figure 5. The absorption rate of the proposed solar cell when (**a**) filling the core with SiO_2 and (**b**) not truncating the cone tip.

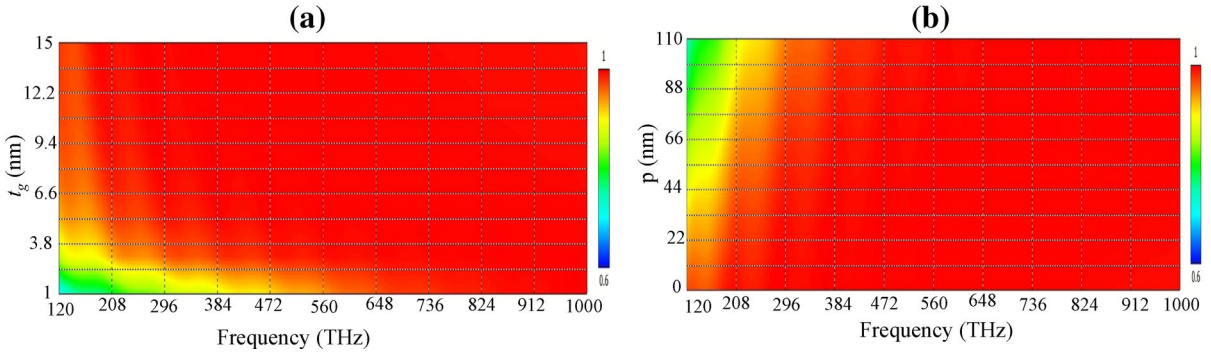

Figure 6. The absorption rate of the proposed solar cell for (**a**) different thicknesses of graphene shell t_g and (**b**) the periodicity of the nano-pillars. The parameter p is the increment in the periodicity from its minimum value $2R_1$ ($T = 2R_1 + p$).

in the size of the system[41]. The reader is referred to the experimental realization of carbon-based hollow particles for high power energy applications as further examples[42–45] Moreover, in Fig. 5b, the impact of tip truncation in the low-frequency absorption improvement is observed.

Parametric analysis. The optical absorption of the proposed device with changes in different geometrical parameters is studied in this section. Initially, let us consider the impact of the thickness of the graphene shell on the absorption rate. The reported absorption manipulation by the increase in the number of wrapped graphene layers around a spherical resonator exhibit different performance for solid silver and dielectric-metal core–shell resonators, respectively increasing and decreasing for thicker shells[30]. As Fig. 6a shows, the mono/few-layer graphene material has a low absorption rate at low frequencies. Thus, the presence of around 10 graphene layers, each with a thickness of 1 nm, is essential for the full spectrum coverage in the proposed device. Note that graphene is essentially a 0.34 nm monolayer of carbon atoms, but inhomogeneities during the fabrication process may result in thicker graphene sheets. For CVD-grown graphene material, treating the monolayer graphene as 1 nm thick effective material is a reasonable choice[46]. Using few-layer graphene films in the optical design, cost, scalability, and ultra-broadband absorption features can be attained but the effective transport of the photothermal energy generated on the surface and the possibility of performance manipulation become limited[11]. Moreover, Fig. 6b investigates the influence of inter-particle distance in the performance and shows that near-field coupling plays a crucial role in the absorption enhancement at lower frequencies since by increasing the distance between the nano-pillars the low-frequency performance is highly affected.

The absorption rate of the proposed solar cell for different cone heights is investigated in Fig. 7. For covering the lower frequencies, the height of the cone should be increased. Since higher frequencies have more energy, the height can be shortened by partially covering the higher frequencies to reach a compact device. With the height of 500 nm (substrate thickness 100 nm), a 90% absorption rate for the frequencies beyond 300 THz can be achieved. The same performance is attained with metal-coated moth-eye films with the same geometry. The cone height and substrate thickness are respectively around 200 nm and 5 μm in this device[47].

Finally, the morphology-dependent behavior of the proposed structure is investigated in Fig. 8. Notably, tapering of individual nano-objects is regarded as a promising strategy to engineer the far-field and near-field optical response of nanostructured metamaterials[48–51]. However, since the nanowire system is relatively easy to realize and control, two simpler geometries are analyzed in the following. Specifically, in Fig. 8a the pyramidal nano-pillar is converted to a cylindrical cavity with the same height and shell thickness and the radius of the cavity is varied from 40 to 120 nm. The absorption rate is large at low (high) frequencies for large (small) radii, as expected. Thus, the absorption rate can be sacrificed to attain a simpler geometry. For the intermediate radius of 80 nm, the absorption rate above 90% in the solar spectrum is attained. Moreover, illustrated in Fig. 8b is

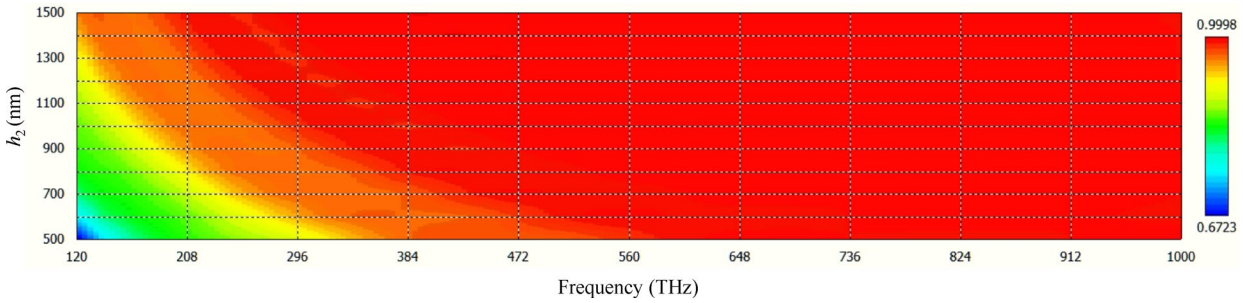

Figure 7. The absorption rate of the proposed solar cell for different cone heights h_2.

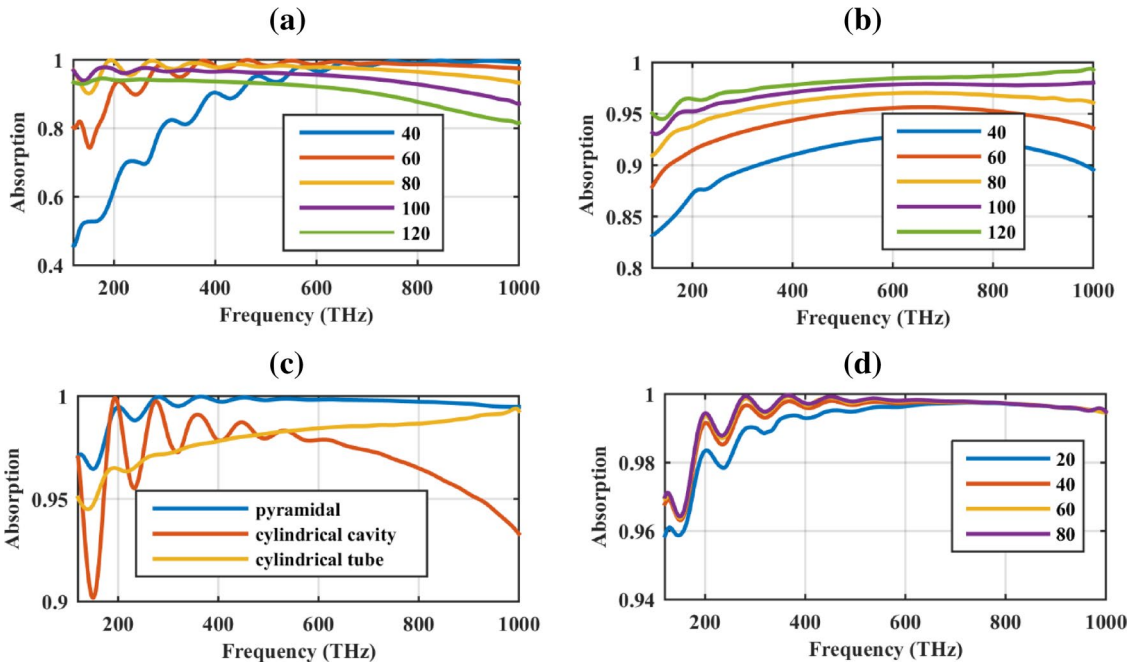

Figure 8. The absorption rate of the cylindrical (**a**) cavity and (**b**) tube for different thicknesses. (**c**) Comparison of the absorption rate of pyramidal solar cell with the optimum cylindrical cavity and tube solar cell. (**d**) The impact of the substrate thickness in the absorption rate of the pyramidal absorber.

the absorption rate of the same structure by converting it to a hollow tube. It is observed that by increasing the tube radius, the absorption increases as well, being above 95% in the solar spectrum for the radius of 120 nm. To further illustrate the priority of the pyramidal geometry, the absorption rate of the pyramidal geometry is compared with those of cylindrical cavity (with the radius 80 nm) and cylindrical tube (with the radius 120 nm) in Fig. 8c. Moreover, the substrate thickness of the pyramidal geometry is varied in Fig. 8d, to confirm that it is chosen properly. Increasing the substrate height beyond 40 nm has a negligible impact on the absorption rate.

Conclusions

With the combined use of shell-shaped graphene-based hollow nano-pillars and a refractory metal substrate, a full-spectrum solar cell is designed. These two sections are respectively responsible for impedance matching and transmission blockage, leading to efficient energy absorption. Moreover, the performance is further explained by exhibiting the azimuthal and longitudinal cavity resonances with different orders in the spectrum. The polarization in-sensitive absorption of the solar cell is maintained up to 65°. Moreover, it is observed that tip truncation and using hollow particles are two key factors for the efficient absorption of the low-frequency waves. The proposed device is heat tolerant and environmentally robust and can be possibly realized by the current fabrication technology.

Methods

The unit cell analysis of CST software is used for simulation[52]. The Floquet ports with two prorogating modes are considered during the simulations. The absorption rate (A) of the structure is calculated using the simulated reflectance (R) and transmittance (T) as[37]:

$$A = 1 - T - R = 1 - |S_{21}|^2 - |S_{11}|^2 \quad (4)$$

where S_{11} and S_{12} are the scattering parameters.

Received: 10 May 2021; Accepted: 26 July 2021
Published online: 09 August 2021

References

1. Liang, H. *et al.* Progress in full spectrum solar energy utilization by spectral beam splitting hybrid PV/T system. *Renew. Sustain. Energy Rev.* **141**, 110785 (2021).
2. Krishnan, A., Das, S., Krishna, S. R. & Khan, M. Z. A. Multilayer nanoparticle arrays for broad spectrum absorption enhancement in thin film solar cells. *Opt. Express* **22**, A800–A811 (2014).
3. Olaimat, M. M., Yousefi, L. & Ramahi, O. M. Using plasmonics and nanoparticles to enhance the efficiency of solar cells: Review of latest technologies. *JOSA B* **38**, 638–651 (2021).
4. Akimov, Y. A. & Koh, W. S. Design of plasmonic nanoparticles for efficient subwavelength light trapping in thin-film solar cells. *Plasmonics* **6**, 155–161 (2011).
5. Yang, Z., Gao, P., Zhang, C., Li, X. & Ye, J. Scattering effect of the high-index dielectric nanospheres for high performance hydrogenated amorphous silicon thin-film solar cells. *Sci. Rep.* **6**, 1–7 (2016).
6. Liang, Q., Duan, H., Zhu, X., Chen, X. & Xia, X. Solar thermal absorber based on dielectric filled two-dimensional nickel grating. *Opt. Mater. Exp.* **9**, 3193–3203 (2019).
7. Kim, I., So, S., Rana, A. S., Mehmood, M. Q. & Rho, J. Thermally robust ring-shaped chromium perfect absorber of visible light. *Nanophotonics* **7**, 1827–1833 (2018).
8. Yu, P. *et al.* Ultra-wideband solar absorber based on refractory titanium metal. *Renew. Energy* **158**, 227–235 (2020).
9. Yu, P. *et al.* A numerical research of wideband solar absorber based on refractory metal from visible to near infrared. *Opt. Mater.* **97**, 109400 (2019).
10. Ren, H. *et al.* Hierarchical graphene foam for efficient omnidirectional solar–thermal energy conversion. *Adv. Mater.* **29**, 1702590 (2017).
11. Lin, K.-T., Lin, H., Yang, T. & Jia, B. Structured graphene metamaterial selective absorbers for high efficiency and omnidirectional solar thermal energy conversion. *Nat. Commun.* **11**, 1–10 (2020).
12. Lin, S. S. *et al.* Stable 16.2% efficient surface plasmon-enhanced graphene/GaAs heterostructure solar cell. *Adv. Energy Mater.* **6**, 1600822 (2016).
13. Won, R. Photovoltaics: Graphene–silicon solar cells. *Nat. Photonics* **4**, 411 (2010).
14. Chen, X., Jia, B., Zhang, Y. & Gu, M. Exceeding the limit of plasmonic light trapping in textured screen-printed solar cells using Al nanoparticles and wrinkle-like graphene sheets. *Light Sci. Appl.* **2**, e92 (2013).
15. Lin, H. *et al.* A 90-nm-thick graphene metamaterial for strong and extremely broadband absorption of unpolarized light. *Nat. Photonics* **13**, 270–276 (2019).
16. Das, S., Sudhagar, P., Kang, Y. S. & Choi, W. Graphene synthesis and application for solar cells. *J. Mater. Res.* **29**, 299–319 (2014).
17. Xiong, H. & Yang, F. Ultra-broadband and tunable saline water-based absorber in microwave regime. *Opt. Express* **28**, 5306–5316 (2020).
18. You, X. *et al.* Ultra-wideband far-infrared absorber based on anisotropically etched doped silicon. *Opt. Lett.* **45**, 1196–1199 (2020).
19. Dorche, A. E., Abdollahramezani, S., Chizari, A. & Khavasi, A. Broadband, polarization-insensitive, and wide-angle optical absorber based on fractal plasmonics. *IEEE Photonics Technol. Lett.* **28**, 2545–2548 (2016).
20. Shen, Y. *et al.* Ultrabroadband terahertz absorption by uniaxial anisotropic nanowire metamaterials. *IEEE Photonics Technol. Lett.* **27**, 2284–2287 (2015).
21. Dang, P. T. *et al.* Efficient broadband truncated-pyramid-based metamaterial absorber in the visible and near-infrared regions. *Curr. Comput.-Aided Drug Des.* **10**, 784 (2020).
22. Liu, Z. *et al.* Truncated titanium/semiconductor cones for wide-band solar absorbers. *Nanotechnology* **30**, 305203 (2019).
23. Falkovsky, L. A. Optical properties of graphene and IV–VI semiconductors. *Phys. Usp.* **51**, 887 (2008).
24. Vakil, A. Transformation optics using graphene: One-atom-thick optical devices based on graphene (2012).
25. Kravets, V. *et al.* Spectroscopic ellipsometry of graphene and an exciton-shifted van Hove peak in absorption. *Phys. Rev. B* **81**, 155413 (2010).
26. Schedin, F. *et al.* Surface-enhanced Raman spectroscopy of graphene. *ACS Nano* **4**, 5617–5626 (2010).
27. Xu, Q. & Huang, Y. Anechoic and reverberation chambers: Theory, design, and measurements (2019).
28. Pflüger, J. & Fink, J. *Handbook of Optical Constants of Solids* 293–311 (Elsevier, New York, 1997).
29. Pflüger, J., Fink, J., Weber, W., Bohnen, K. & Crecelius, G. Dielectric properties of TiC x, TiN x, VC x, and VN x from 1.5 to 40 eV determined by electron-energy-loss spectroscopy. *Phys. Rev. B* **30**, 1155 (1984).
30. Wan, M. *et al.* Strong tunable absorption enhancement in graphene using dielectric-metal core-shell resonators. *Sci. Rep.* **7**, 1–10 (2017).
31. Chirumamilla, M. *et al.* Large-area ultrabroadband absorber for solar thermophotovoltaics based on 3D titanium nitride nanopillars. *Adv. Opt. Mater.* **5**, 1700552 (2017).
32. Verre, R., Odebo Länk, N., Andrén, D., Šípová, H. & Käll, M. Large-scale fabrication of shaped high index dielectric nanoparticles on a substrate and in solution. *Adv. Opt. Mater.* **6**, 1701253 (2018).
33. Hajati, M. & Hajati, Y. Plasmonic characteristics of two vertically coupled graphene-coated nanowires integrated with substrate. *Appl. Opt.* **56**, 870–875 (2017).
34. Chen, B. *et al.* Graphene coated ZnO nanowire optical waveguides. *Opt. Express* **22**, 24276–24285 (2014).
35. Huang, Z., Zhong, P., Wang, C., Zhang, X. & Zhang, C. Silicon nanowires/reduced graphene oxide composites for enhanced photoelectrochemical properties. *ACS Appl. Mater. Interfaces* **5**, 1961–1966 (2013).
36. Cai, D. *et al.* Facile synthesis of ultrathin-shell graphene hollow spheres for high-performance lithium-ion batteries. *Electrochim. Acta* **139**, 96–103 (2014).
37. Raad, S. H. & Atlasbaf, Z. Broadband continuous/discrete spectrum optical absorber using graphene-wrapped fractal oligomers. *Opt. Express* **28**, 18049–18058 (2020).
38. Aalizadeh, M., Khavasi, A., Serebryannikov, A. E., Vandenbosch, G. A., & Ozbay, E. A route to unusually broadband plasmonic absorption spanning from visible to mid-infrared. *Plasmonics* **14**(5), 1269-1281 (2019).
39. Ozel, T. *et al.* Electrochemical deposition of conformal and functional layers on high aspect ratio silicon micro/nanowires. *Nano Lett.* **17**, 4502–4507 (2017).
40. Fallahzadeh, S., Forooraghi, K. & Atlasbaf, Z. Design, simulation and measurement of a dual linear polarization insensitive planar resonant metamaterial absorber. *Prog. Electromagn. Res. Lett.* **35**, 135–144 (2012).
41. Yang, B., Wu, T., Yang, Y. & Zhang, X. Tunable subwavelength strong absorption by graphene wrapped dielectric particles. *J. Opt.* **17**, 035002 (2015).

42. Huang, Q. *et al.* Hollow carbon nanospheres with extremely small size as anode material in lithium-ion batteries with outstanding cycling stability. *J. Phys. Chem. C* **120**, 3139–3144 (2016).
43. Liu, T., Zhang, L., Cheng, B. & Yu, J. Hollow carbon spheres and their hybrid nanomaterials in electrochemical energy storage. *Adv. Energy Mater.* **9**, 1803900 (2019).
44. Shao, Q. *et al.* Synthesis and characterization of graphene hollow spheres for application in supercapacitors. *J. Mater. Chem. A* **1**, 15423–15428 (2013).
45. Thangavel, R. *et al.* Highly interconnected hollow graphene nanospheres as an advanced high energy and high power cathode for sodium metal batteries. *J. Mater. Chem. A* **6**, 9846–9853 (2018).
46. Zhu, X. *et al.* Enhanced light–matter interactions in graphene-covered gold nanovoid arrays. *Nano Lett.* **13**, 4690–4696 (2013).
47. Nakamura, Y., Toma, M. & Kajikawa, K. A visible and near-infrared broadband light absorber of cone-shaped metallic cavities. *Appl. Phys. Express* **13**, 062001 (2020).
48. Zagaglia, L., Demontis, V., Rossella, F. & Floris, F. Semiconductor nanowire arrays for optical sensing: A numerical insight on the impact of array periodicity and density. *Nanotechnology* **32**, 335502 (2021).
49. Floris, F. *et al.* Strong modulations of optical reflectance in tapered core-shell nanowires. *Materials* **12**, 3572 (2019).
50. Floris, F. *et al.* Self-assembled InAs nanowires as optical reflectors. *Nanomaterials* **7**, 400 (2017).
51. Demontis, V., Marini, A., Floris, F., Sorba, L. & Rossella, F. in *AIP Conference Proceedings*. 020009 (AIP Publishing LLC).
52. https://www.3ds.com/products-services/simulia/products/cst-studio-suite.

Acknowledgements

This work was supported by Iran's National Science Foundation (INSF) under Contract 98012903.

Author contributions

S.H.R. proposed the idea, performed the simulations, and wrote the initial draft. Z.A. supervised the entire project. All authors confirmed the final manuscript.

Competing interests

The authors declare no competing interests.

Additional information

Correspondence and requests for materials should be addressed to S.H.R.

Reprints and permissions information is available at www.nature.com/reprints.

Publisher's note Springer Nature remains neutral with regard to jurisdictional claims in published maps and institutional affiliations.